

Understanding the Strong Apparent Injection Dependence of Carrier Lifetimes in Doped Polycrystalline Silicon Passivated Wafers

Rabin Basnet,* Di Yan, Pheng Phang, Thien Truong, Di Kang, Heping Shen, and Daniel Macdonald

This study investigates the injection dependence of carrier lifetimes of p- and n-type samples passivated by doped-polycrystalline silicon (poly-Si) (p^+ and n^+ poly-Si) contacts. A strong apparent injection dependence of the carrier lifetimes is observed in p-n junction samples (p^+ poly-Si on n-type or n^+ poly-Si on p-type) but no injection dependence is observed in high-low junction samples (p^+ poly-Si on p-type or n^+ poly-Si on n-type). Further, photoluminescence images captured at two illumination intensities of 0.05 and 0.87 suns reveal that edge recombination contributed the strong apparent injection dependence in p-n junction samples. Furthermore, this apparent injection dependence increases as the sample size is reduced, and as the sheet resistance of the doped poly-Si contacts is decreased, allowing more effective transport of minority carriers to the recombination-active edge regions.

values (single-side) of $7\text{--}15 \text{ fA cm}^{-2}$.^[2,6-9] Moreover, progress in the electronic quality of silicon wafers (both n-and p-type) has yielded high bulk lifetimes,^[10,11] leading to consistent demonstration of doped-poly-Si solar cells with efficiencies greater than 25%.^[12-16]

Understanding and modelling the performance of solar cells necessitates knowledge of injection-dependent carrier lifetimes. It is widely recognized that strongly injection-dependent carrier lifetimes can negatively impact solar cell performance (mostly fill factor), particularly at lower illumination intensities (<1 sun).^[17,18] Their presence can be attributed to recombination centres originating from various sources, including: i)

level defects in the silicon bulk, such as the boron–oxygen (B–O) complex, metal impurities, and oxygen precipitate-related defects;^[19-21] ii) the presence of surface defects or dielectric layers (AlO_x and SiN_x) with high fixed charge densities;^[22-24] and iii) edge recombination.^[22,24,25]

Chen et al.^[25] demonstrated that the presence of edge recombination and localized recombination increases the apparent injection dependence of carrier lifetimes in a manner that appears similar to Shockley–Read–Hall recombination. Hameiri et al.^[22] through a comprehensive investigation, elucidated the influence of surface damage regions and edge recombination on the injection dependence in both p-and n-type samples, passivated by dielectric films. Their study suggested that the fixed charge associated with the AlO_x and SiN_x layers contributes to the strong injection dependence of carrier lifetimes of the samples when a surface damage region and edge recombination is present on the samples. Further, Cattin et al.^[17] also reported a strong injection dependence of carrier lifetimes in samples passivated by amorphous silicon stacks used in silicon heterojunction solar cells. Their study revealed that localized surface defects can have a detrimental effect on well-passivated regions located several centimetres away, through electrical connection by the electrode. This results in a drop in low-injection lifetime after electrode deposition. Consequently, the commonly measured injection-dependent lifetimes prior to metallization often fail to accurately represent the device post-metallization. Furthermore, Veith et al.^[24] also reported the strong injection dependence of the effective carrier

1. Introduction

Doped-polycrystalline silicon (poly-Si) passivating contacts have emerged as a key technology for the next generation of silicon solar cells in mass production, owing to their excellent performance and high compatibility with the existing passivated emitter and rear cell (PERC) technology.^[1] Phosphorus-doped poly-Si contacts, regardless of the interfacial oxide growth method and the technique employed for poly-Si deposition, typically exhibit a recombination current density (J_0) within the range of $1\text{--}5 \text{ fA cm}^{-2}$ (single-side).^[2-5] While the passivation performance of p^+ poly-Si contacts generally do not match that of n^+ poly-Si contacts, they still attain typical J_0

R. Basnet, P. Phang, T. Truong, D. Kang, H. Shen, D. Macdonald
School of Engineering

The Australian National University
Canberra, ACT 2601, Australia
E-mail: rabin.basnet@anu.edu.au

D. Yan
Department of Electrical and Electronic Engineering
University of Melbourne
Melbourne, Victoria 3010, Australia

T. Truong
National Renewable Energy Laboratory (NREL)
15103 Denver West Pkwy., Golden, CO 80401, USA

 The ORCID identification number(s) for the author(s) of this article can be found under <https://doi.org/10.1002/solr.202400087>.

DOI: 10.1002/solr.202400087

lifetime due to the formation of inversion layer when AlO_x layers passivated n -type wafers. Their study showed the size of the samples also has an impact on the degree of injection dependence of carrier lifetimes. Therefore, it is necessary to use sufficiently large samples when evaluating the apparent injection dependence of carrier lifetimes.

Several recent works have also reported strong apparent injection-dependent carrier lifetimes in both n - and p -type samples passivated by p^+ poly-Si contacts.^[11,26–29] Given the high-quality wafers and the excellent surface passivation offered by doped poly-Si contacts, a comprehensive investigation of the mechanisms behind this observed strong apparent injection-dependent minority carrier lifetimes is necessary.

2. Results and Discussion

2.1. Doped poly-Si passivation

Figure 1 shows the injection-dependent carrier lifetimes of n -type (FZ- $2\Omega\text{cm}^{-1}$) and p -type (boron-doped FZ- $1.8\Omega\text{cm}^{-1}$) samples passivated by p^+ poly-Si contacts and n^+ poly-Si contacts. The injection dependency of carrier lifetimes of the samples reveals two distinct trends. The samples with a p-n junction (p^+ poly-Si on n -type or n^+ poly-Si on p -type) show strongly injection-dependent carrier lifetimes, particularly evident at excess minority carrier densities $< 2 \times 10^{15}\text{ cm}^{-3}$. However, the samples with a high-low junction (p^+ poly-Si on p -type or n^+ poly-Si on n -type) do not show any noticeable injection-dependent carrier lifetimes at excess minority carrier densities $< 2 \times 10^{15}\text{ cm}^{-3}$. Note, we observed a similar behaviour in Ga-doped p -type Czochralski silicon samples, as shown in **Figure S1**, Supporting Information.

Further, PL images of these four samples were captured under two illumination intensities of 0.87 and 0.05 suns, as shown in **Figure 2a,b**. At 0.05 suns illumination intensity, the PL images

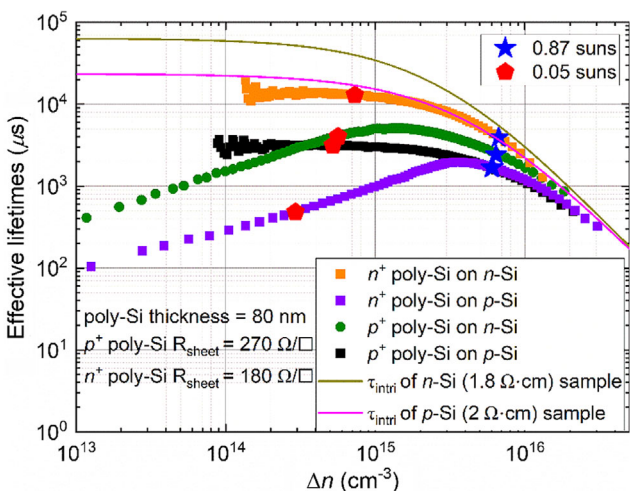


Figure 1. Injection-dependent carrier lifetimes of n -type (FZ) and p -type (FZ) samples passivated by p^+ and n^+ poly-Si contacts. The excess carrier densities corresponding to 0.87 and 0.05 suns are marked by solid stars and pentagons, respectively. Note the carrier lifetimes were measured on quarters of 4 inch wafers.

reveal that only the p-n junction samples exhibit a strong edge recombination, as shown in **Figure 2a**. Note we used 80 nm thick intrinsic poly-Si layers for both n^+ and p^+ doped poly-Si contacts, resulting in sheet resistances of achieved 180 and $270\Omega/\square$, respectively. Interestingly, the high edge recombination appears to be in n^+ poly-Si on p-Si samples (more than 2 cm) compared to p^+ poly-Si on n-Si (up to 1 cm), which could be attributed to low sheet resistance of n^+ poly-Si contacts. Furthermore, line scans clearly indicate that the extent of edge recombination extends in the p-n junction samples, as shown in **Figure 2c**. However, at 0.87 suns illumination intensity, the edge recombination is not evident in both types of samples as shown by PL images and corresponding line scans in **Figure 2b,d**. This observation suggests a direct correlation between the apparent injection dependency of carrier lifetimes and the presence of a p-n junction samples.

2.2. Edge Recombination

Next, we explored the role of edge recombination in the injection dependence of carrier lifetimes, particularly in relation to the sample size. To comprehensively investigate the role of edge recombination, we used p^+ poly-Si contacts to form a high-low junction with p -type (FZ) samples and a p-n junction with n -type (FZ) samples. Initially, measurements were conducted on the “full” samples, referring to 4 inch samples with their centre positioned on the sensing coil of the QSSPC system. Interestingly, the “full” samples for both n -type and p -type samples exhibited relatively weak injection-dependent carrier lifetimes, as shown in **Figure 3a,b**. Subsequently, the lifetimes were measured following the cleavage of samples into halves and quarters. Notably, for both the “half” and “quarter” samples, the injection dependence of carrier lifetimes of the p-FZ samples did not change, but the n -type samples exhibited increasingly stronger injection dependency in the carrier lifetimes, as shown in **Figure 3a,b**. This is consistent with the behaviour of edge recombination in PERC solar cells which shows the strong correlation with the sample size.^[30]

Further, the calculated diffusion length of minority carriers for the p -type samples (electrons) and n -type samples (holes) was estimated to be 3.3 and 2.2 mm at an excess carrier density of $5 \times 10^{14}\text{ cm}^{-3}$ respectively, which are quite similar. This observation suggests that the difference in behaviour between the p-n junction and high-low junction samples is not attributed to the diffusion length, but rather to the transport of carriers toward the edges. Specifically, for the p-n junction samples, the doped poly-Si (p^+ poly-Si) contacts established a conductive pathway for minority charge carriers (in this case holes) to reach the edges, even over considerable distances of centimetres.^[24] Therefore, the smaller the sample area, the larger the impact of edge recombination, as shown in the PL images in **Figure S2**, Supporting Information. However, this conductive path for minority carriers is not available in the high-low junction samples, reducing the lateral impact of the edge recombination. Further, similar phenomenon was observed when we introduced the localized surface damage recombination by intentionally induced scratch using diamond scriber, as shown in the PL images in **Figure S3**, Supporting Information.

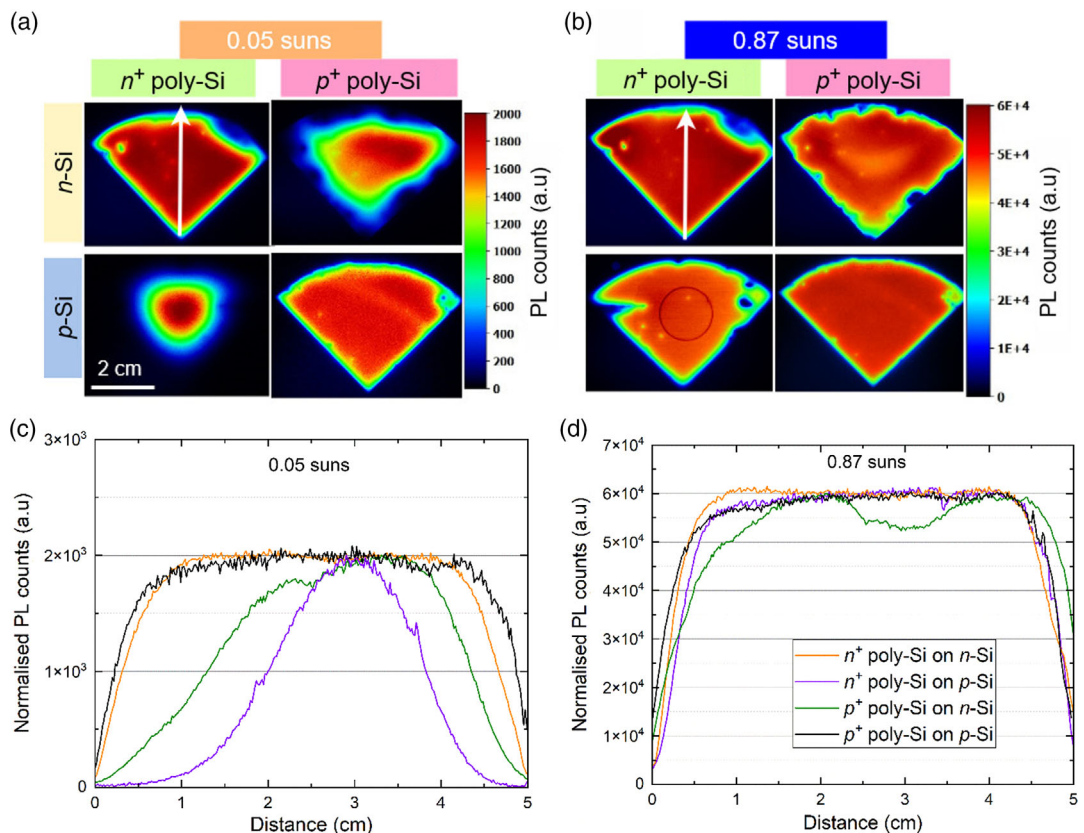


Figure 2. Normalised PL images of the n- and p-type samples passivated by n^+ and p^+ poly-Si contacts captured at two different illumination intensities of a) 0.05 suns and b) 0.87 suns. Line scans of normalised PL images of samples captured at c) 0.05 suns and d) 0.87 suns. The white arrows in Figure a and b) indicate line scan direction.

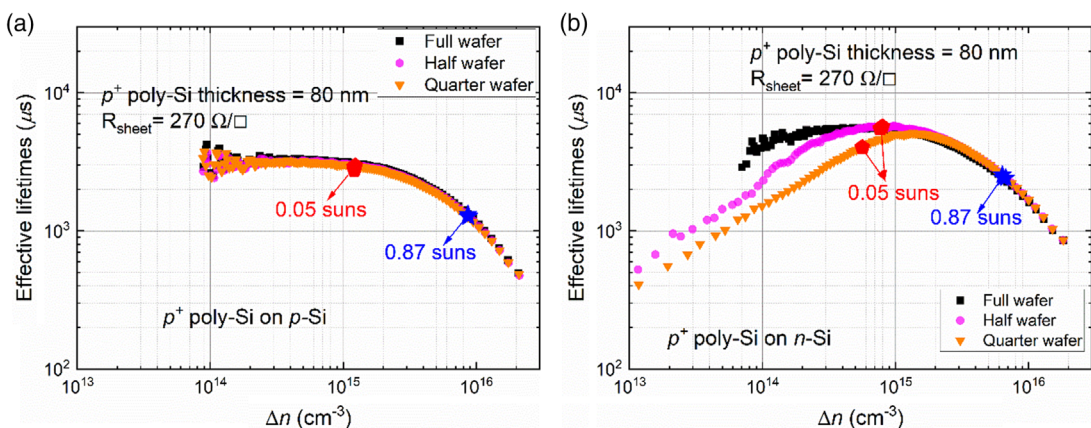


Figure 3. a) Injection-dependent carrier lifetimes of the a) p -type samples and b) n -type samples passivated by p^+ poly-Si contacts. The excess carrier densities corresponding to 0.87 and 0.05 suns are marked by stars and pentagons, respectively. The passivation was initially applied on full wafers (4 inch) and then the samples were cleaved into halves and subsequently quarters.

The negligible injection dependence of carrier lifetimes found in our high-low junction samples (p -type FZ or CZ) contradicts the findings of previous works.^[11,27] Those investigations reported a strong injection-dependent carrier lifetime in p -type samples passivated by both intrinsic (hydrogenated) and p^+ poly-Si contacts. This discrepancy may be attributed to the

high-quality wafers (FZ or CZ) and the pre-treatment step used in this work which mitigated bulk SRH recombination related either to grown-in vacancy^[31] or oxygen precipitates defects.^[32] It may also be caused by local damaged on the samples, such as during fabrication or handling. Nevertheless, we found that the degree of injection dependency of carrier lifetimes can be

slightly reduced by deposition of passivating layers such as AlO_x , which wraps around the edges.

2.3. Sheet Resistance

We also investigated the impact of the sheet resistance of the doped poly-Si layers on the apparent injection dependence of carrier lifetimes in the p-n junction samples. To explore this, we again passivated n-type samples with p^+ poly-Si contacts of varying sheet resistances (R_{sheet}): 170, 270, and $370 \Omega/\square$. This was achieved by varying intrinsic poly-Si film thicknesses: 120, 80, and 50 nm, respectively, and subjecting them to the same boron diffusion conditions. It is worth noting that the final thickness of the doped poly-Si contacts might have slightly decreased due to the formation of a boron silicate glass layer during the diffusion process. The boron concentration profiles of p^+ poly-Si contacts of these three samples are shown in Figure S5, Supporting Information. **Figure 4** shows the injection dependence of apparent carrier lifetimes of three samples passivated by p^+ poly-Si contacts with three different R_{sheet} of 170, 270, and $370 \Omega/\square$. The impact of edge recombination becomes more prominent as the R_{sheet} of the p^+ poly-Si layers decrease. In the case of p^+ poly-Si passivated samples with R_{sheet} of $170 \Omega/\square$ (Figure 4a), a stronger injection-dependent lifetime is evident even when measured on a full wafer, and this injection

dependence becomes stronger as the sample size is reduced. In contrast, the poly-Si passivated samples with R_{sheet} of $370 \Omega/\square$ do not exhibit any obvious injection dependence on carrier lifetimes (Figure 4c). Furthermore, we observed that when R_{sheet} increased from 170 to $270 \Omega/\square$, the apparent carrier lifetime started to show a strong injection dependence at slightly low injection level ($1 \times 10^{15} \text{ cm}^{-3}$) compared to previously at $2 \times 10^{15} \text{ cm}^{-3}$ (for quarter samples). This observation implies as the R_{sheet} of doped poly-Si contacts is reduced, the lateral transport of minority carriers becomes more efficient,^[33] thus amplifying the impact of edge recombination. We also note that this injection dependence of apparent carrier lifetimes are dependent on the sample resistivity as discussed in Figure S4, Supporting Information.

Finally, we carefully etched back the p^+ poly-Si contacts (n-type samples) using Tetramethylammonium hydroxide, followed by an HF dip while retaining the in-diffused boron layers. This process maintained the p-n junction sample, albeit with a significantly higher sheet resistance of $> 600 \Omega/\square$. The boron concentration profile of p^+ poly-Si contacts is shown in Figure S6, Supporting Information. The sample was then re-passivated using thermal AlO_x layers deposited by atomic layer deposition (ALD). **Figure 5a** shows a comparison of the injection-dependent carrier lifetimes of the same sample when passivated by p^+ poly-Si contacts and AlO_x layers. Interestingly, the carrier lifetime of

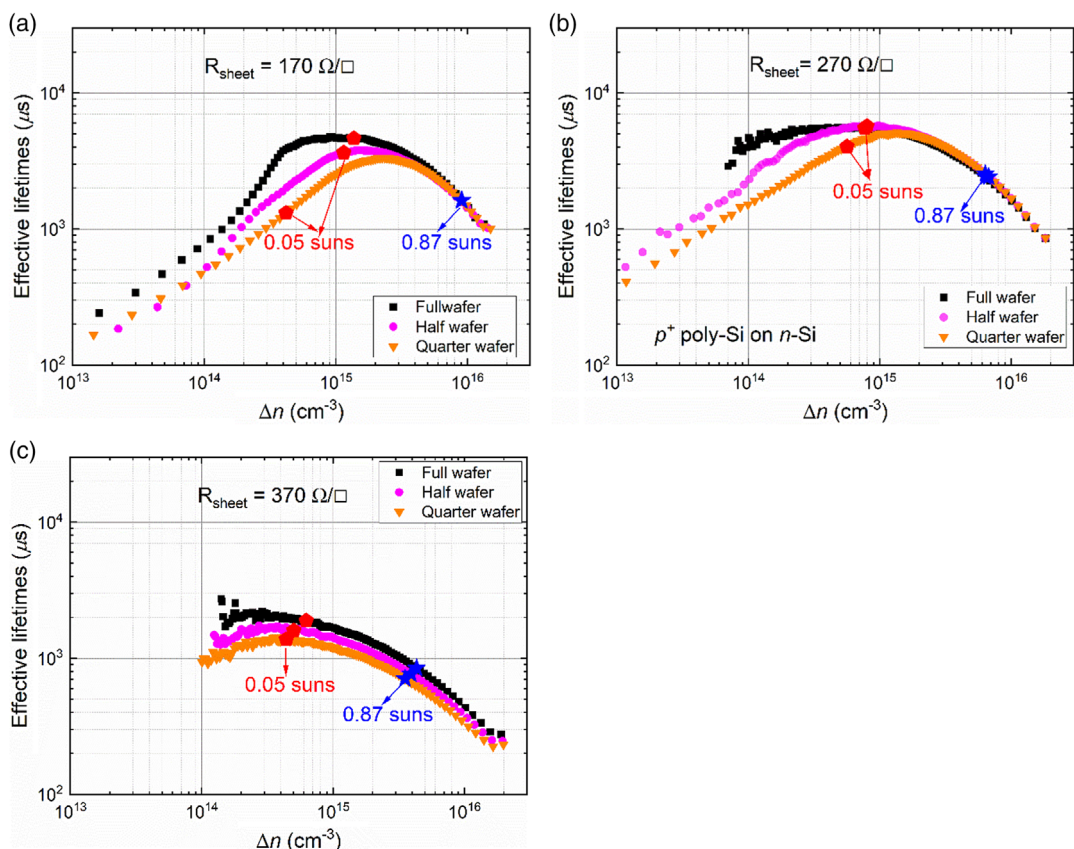


Figure 4. Injection-dependent carrier lifetimes of n-type samples ($2 \Omega \text{ cm}^{-1}$) passivated by p^+ poly-Si passivated contacts with R_{sheet} of a) $170 \Omega/\square$, b) $270 \Omega/\square$, and c) $370 \Omega/\square$. The injection levels corresponding to 0.87 and 0.05 suns are marked by solid stars and pentagons, respectively. The passivation was started with full wafers (4 inch) and then the samples were cleaved into halves and subsequently quarters.

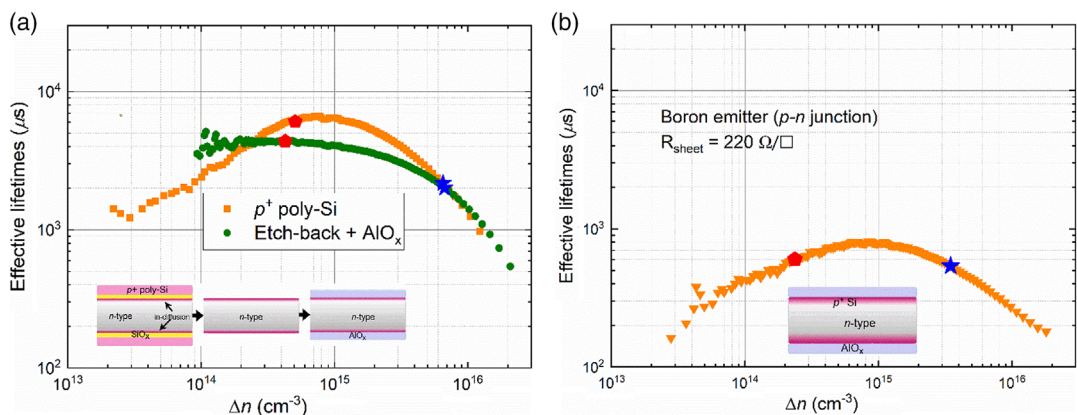


Figure 5. a) Injection-dependent carrier lifetime of an *n*-type sample passivated by p^+ poly-Si contacts and after etching the p^+ poly-Si layers and re-passivating with AlO_x layers. b) Injection-dependent apparent carrier lifetime of *n*-type sample with boron diffusion (p^+ -Si) and passivated by AlO_x layers.

the same sample after AlO_x passivation ($J_0 = 7.2 \text{ fA cm}^{-2}$) no longer exhibits a strong injection dependence, as expected due to the high sheet resistance. Furthermore, we also diffused boron on an *n*-type sample creating a p-n junction without poly-Si contacts with a sheet resistance of $220 \Omega/\square$, and subsequently passivated them by thermal AlO_x layers. Figure 5b shows the strong apparent injection dependence of carrier lifetimes of this sample. These observations further demonstrate that the apparent injection-dependent carrier lifetimes in p-n junction depend on the sheet resistance of the diffused junction which affects the lateral transport of minority charge carriers. This phenomenon aligns with previous observation made in homojunction devices^[34] and heterojunction devices.^[17,35] Therefore, this apparent injection dependence of carrier lifetimes would be similar irrespective how the p-n junctions are formed, either via thermal diffusion, doped poly-Si contacts, or silicon heterojunctions. As a result, a reduction in the fill factor is expected if p-n junction formed by poly-Si passivating contacts is used in solar cells, such as in rear junctions or poly-Si based interdigitated back contacted structures. This requires further optimization when designing solar cells where p-n junctions are formed by doped poly-Si contacts, particularly when half-cut cells (or shingles) are used for module fabrication. The optimization process should primarily focus on edge passivation, which has been demonstrated by using AlO_x layers.^[36]

3. Conclusion

In summary, this work investigates the strong apparent injection dependence of carrier lifetimes of the samples (*n*- and *p*-type) passivated by doped poly-Si (n^+ and p^+ poly-Si) contacts. The influence of edge recombination on effective carrier lifetimes was found to be negligible in high-low junction samples, in contrast to the observed strong injection-dependent carrier lifetimes in p-n junction samples, in which the junction provides a conductive path for minority carrier to be effectively transported to the recombination-active edges, over distances of centimetres. The apparent injection dependence varied depending on factors such as sample size and the sheet resistance of the doped poly-Si

contacts. With the next generation of doped poly-Si based solar cells expected to adopt rear junction, interdigitated back contact or bi-poly-Si structures, this study emphasizes that edge recombination has minimal impact on open circuit voltage (under 1 sun). However, it could influence the fill factor, particularly under lower illumination intensity, especially for smaller wafer sizes or those with lower sheet resistance.

4. Experimental Section

This work utilizes 4 inch round *n*- and *p*-type electronic-grade float zone (FZ) silicon samples with resistivity of $1.8 - 2$ and $100 \Omega \text{ cm}^{-1}$ *n*-type FZ. Unless specified, the poly-Si contacts were formed on the quarter of 4 inch samples. The RCA-cleaned samples were subjected to a high-temperature pre-treatment at 1050°C for 30 min in an oxygen ambient to enhance the bulk quality.^[31,32] After a subsequent cycle of chemical cleaning, ultrathin SiO_x layers were grown by thermal oxidation in a quartz tube furnace at 600°C for 5 min. Then, the deposition of intrinsic poly-Si films was performed in a low-pressure chemical vapour deposition system, using pure silane gas at a temperature of 530°C and at a pressure of 250 mTorr . Three different poly-Si film thicknesses (50, 80, and 120 nm) were deposited on the samples. The film thickness was measured using a JA Woollam M2000D ellipsometer.

All the intrinsic poly-Si deposited samples were pre-annealed at 1000°C for 1 h in a nitrogen ambient prior to dopant diffusions to improve the passivation of poly-Si contacts (particularly p^+ poly-Si contacts) by promoting stoichiometry of the interfacial oxides.^[37] Subsequently, some of the 80 nm thick intrinsic poly-Si samples (*n*- and *p*-type wafers) underwent phosphorus diffusion at 800°C for 40 min with phosphorus oxychloride (POCl_3) as dopant source followed by a 10 min drive-in annealing in nitrogen to form n^+ poly-Si contacts, resulting in a sheet resistance of $180 \Omega/\square$. The remaining samples (*n*- and *p*-type wafers), with 50, 80, and 120 nm thick poly-Si films were subjected to boron diffusion at 880°C for 25 min with boron tribromide (BBBr_3) as dopant source followed by a 25 min drive-in annealing in nitrogen to form p^+ poly-Si contacts.

Effective carrier lifetimes were measured using the quasi-steady state photoconductance and transient photoconductance decay techniques with a WCT-120 tool from Sinton Instruments (software version V4.5.0).^[38] The recombination current density (J_0) values were determined at an injection level of $1 \times 10^{16} \text{ cm}^{-3}$ using the Kane and Swanson^[39] method based on high resistivity ($100 \Omega \text{ cm}^{-1}$) *n*-type FZ samples with symmetrical doped poly-Si structures. PL images were captured using an LIS-R1 PL imaging tool from BT imaging.^[40]

Supporting Information

Supporting Information is available from the Wiley Online Library or from the author.

Acknowledgements

This work has been supported by the Australian Renewable Energy Agency (ARENA) through the Australian Centre for Advanced Photovoltaics (ACAP), and project 2022/TRAC004 and 2022/TRAC005.

Conflict of Interest

The authors declare no conflict of interest.

Data Availability Statement

The data that support the findings of this study are available from the corresponding author upon reasonable request.

Keywords

doped poly-Si passivating contacts, edge recombination, injection-dependent carrier lifetimes, solar cells, TOPCon

Received: January 31, 2024

Revised: May 13, 2024

Published online: May 28, 2024

- [1] VDMA, in *International Technology Roadmap for Photovoltaic (ITRPV)*, VDMA 2023.
- [2] R. Peibst, Y. Larionova, S. Reiter, M. Turcu, R. Brendel, D. Tetzlaff, J. Krügener, T. Wietler, U. Höhne, J.-D. Kähler, S. F. H. Mehlich, in *32nd European Photovoltaic Solar Energy Conf. and Exhibition*, Munich, Germany, 2016: pp. 323–327.
- [3] M. K. Stodolny, M. Lenes, Y. Wu, G. J. M. Janssen, I. G. Romijn, J. R. M. Luchies, L. J. Geerligs, *Sol. Energy Mater. Sol. Cells* **2016**, *158*, 24.
- [4] B. Liao, W. Wu, R. J. Yeo, X. Wu, S. Ma, Q. Wang, Y. Wan, X. Su, W. Shen, X. Li, W. Li, G. Xing, B. Hoex, *Prog. Photovoltaics Res. Appl.* **2023**, *31*, 220.
- [5] Y. Huang, M. Liao, Z. Wang, X. Guo, C. Jiang, Q. Yang, Z. Yuan, D. Huang, J. Yang, X. Zhang, Q. Wang, H. Jin, M. Al-Jassim, C. Shou, Y. Zeng, B. Yan, J. Ye, *Sol. Energy Mater. Sol. Cells* **2020**, *208*, 110389.
- [6] A. Merkle, S. Seren, H. Knauss, B. Min, J. Steffens, B. Terheiden, R. Brendel, R. Peibs, in *35th European Photovoltaic Solar Energy Conf. and Exhibition*, Brussels, Belgium 2018, pp. 785–791.
- [7] G. Nogay, J. Stuckelberger, P. Wyss, E. Rucavado, C. Allebé, T. Koida, M. Morales-Masis, M. Despeisse, F.-J. Haug, P. Löper, C. Ballif, *Sol. Energy Mater. Sol. Cells* **2017**, *173*, 18.
- [8] A. Morisset, R. Cabal, B. Grange, C. Marchat, J. Alvarez, M.-E. Gueunier-Farret, S. Dubois, J.-P. Kleider, *Sol. Energy Mater. Sol. Cells* **2019**, *200*, 109912.
- [9] D. Yan, A. Cuevas, J. Bullock, Y. Wan, C. Samundsett, *Sol. Energy Mater. Sol. Cells* **2015**, *142*, 75.
- [10] B. Steinhauser, T. Niewelt, A. Richter, R. Eberle, M. C. Schubert, *Sol. RRL* **2021**, *5*, 2100605.
- [11] Z. Rui, Y. Zeng, X. Guo, Q. Yang, Z. Wang, C. Shou, W. Ding, J. Yang, X. Zhang, Q. Wang, H. Jin, M. Liao, S. Huang, B. Yan, J. Ye, *Sol. Energy* **2019**, *194*, 18.
- [12] A. Richter, J. Benick, F. Feldmann, A. Fell, B. Steinhauser, J.-I. Polzin, N. Tucher, J. N. Murthy, M. Hermle, S. W. Glunz, in *36th European Photovoltaic Solar Energy Conf. and Exhibition*, Marseille, France 2019.
- [13] A. Richter, R. Müller, J. Benick, F. Feldmann, B. Steinhauser, C. Reichel, A. Fell, M. Bivour, M. Hermle, S. W. Glunz, *Nat. Energy* **2021**, *6*, 429.
- [14] JinkoSolar Press Release, JinkoSolar's high-efficiency n-type monocrystalline silicon solar cell sets our new record with maximum conversion efficiency of 26.4%, 2022, <https://ir.jinkosolar.com/news-releases/news-release-details/jinkosolars-high-efficiency-n-type-monocrystalline-silicon-2> (accessed: April 2024).
- [15] Longi Press Release, LONGi sets record of 25.09% for N-Type TOPCon cell efficiency, 2021, <https://www.longi.com/en/news/7477/> (accessed: April 2024).
- [16] Trina Press Release, Trina Solar breaks world record yet again by setting i-TOPCon cell efficiency at 25.5%, 2022, <https://www.trinasolar.com/en-gb/resources/newsroom/trina-solar-breaks-world-record-yet-again-setting-i-topcon-cell-efficiency-255> (accessed: April 2024).
- [17] J. Cattin, J. Haschke, C. Ballif, M. Boccard, *Appl. Phys. Lett.* **2020**, *116*, 113901.
- [18] B. Vermang, E. Cornagliotti, V. Prajapati, J. John, J. Poortmans, R. Mertens, *Phys. Status Solidi RRL* **2012**, *6*, 259.
- [19] K. Bothe, J. Schmidt, *J. Appl. Phys.* **2006**, *99*, 13701.
- [20] D. Macdonald, A. Cuevas, J. Wong-Leung, *J. Appl. Phys.* **2001**, *89*, 7932.
- [21] J. D. Murphy, R. E. McGuire, K. Bothe, V. V. Voronkov, R. J. Falster, *Sol. Energy Mater. Sol. Cells* **2014**, *120*, 402.
- [22] Z. Hameiri, F.-J. Ma, *J. Appl. Phys.* **2015**, *117*, 085705.
- [23] M. Kessler, T. Ohrdes, P. P. Altermatt, R. Brendel, *J. Appl. Phys.* **2012**, *111*, 54508.
- [24] B. Veith, T. Ohrdes, F. Werner, R. Brendel, P. P. Altermatt, N.-P. Harder, J. Schmidt, *Sol. Energy Mater. Sol. Cells* **2014**, *120*, 436.
- [25] F. W. Chen, J. E. Cotter, M. D. Abbott, T.-T. A. Li, K. C. Fisher, *IEEE Trans. Electron Devices* **2007**, *54*, 2960.
- [26] U. Romer, R. Peibst, T. Ohrdes, B. Lim, J. Krugener, T. Wietler, R. Brendel, *IEEE J. Photovoltaics* **2015**, *5*, 507.
- [27] Y. Zhi, J. Zheng, M. Liao, W. Wang, Z. Liu, D. Ma, M. Feng, L. Lu, S. Yuan, Y. Wan, B. Yan, Y. Wang, H. Chen, M. Yao, Y. Zeng, J. Ye, *Sol. Energy Mater. Sol. Cells* **2021**, *230*, 111229.
- [28] L. Lu, Y. Zeng, M. Liao, J. Zheng, Y. Lin, M. Feng, Y. Zhi, H. He, W. Ding, C. Shou, G. Qin, B. Yan, J. Ye, *Sol. Energy Mater. Sol. Cells* **2021**, *223*, 110970.
- [29] X. Guo, M. Liao, Z. Rui, Q. Yang, Z. Wang, C. Shou, W. Ding, X. Luo, Y. Cao, J. Xu, L. Fu, Y. Zeng, B. Yan, J. Ye, *Sol. Energy Mater. Sol. Cells* **2020**, *210*, 110487.
- [30] A. Fell, P. P. Altermatt, *IEEE J. Photovoltaics* **2018**, *8*, 1443.
- [31] N. E. Grant, V. P. Markevich, J. Mullins, A. R. Peaker, F. Rougieux, D. Macdonald, J. D. Murphy, *Phys. Status Solidi* **2016**, *213*, 2844.
- [32] R. Basnet, F. E. Rougieux, C. Sun, S. P. Phang, C. Samundsett, R. Einhaus, J. Degoulange, D. Macdonald, *IEEE J. Photovoltaics* **2018**, *8*, 990.
- [33] A. Fell, J. Schon, M. Muller, N. Wohrle, M. C. Schubert, S. W. Glunz, *IEEE J. Photovoltaics* **2018**, *8*, 428.
- [34] S. Steingrube, O. Breitenstein, K. Ramspeck, S. Glunz, A. Schenk, P. P. Altermatt, *J. Appl. Phys.* **2011**, *110*, 14515.
- [35] F. Gérenton, J. Eymard, S. Harrison, R. Clerc, D. Muñoz, *Sol. Energy Mater. Sol. Cells* **2020**, *204*, 110213.
- [36] B. Martel, M. Albaric, S. Harrison, F. Dhainaut, T. Desrues, *Sol. Energy Mater. Sol. Cells* **2023**, *250*, 112095.

- [37] J. Stuckelberger, D. Yan, S. P. Phang, C. Samundsett, J. Wang, L. Antognini, F.-J. Haug, Z. Wang, J. Yang, P. Zheng, X. Zhang, D. Macdonald, *Sol. Energy Mater. Sol. Cells* **2023**, *251*, 112123.
- [38] R. A. Sinton, A. Cuevas, *Appl. Phys. Lett.* **1996**, *69*, 2510.
- [39] D. E. Kane, R. M. Swanson, in *Measurement of the Emitter Saturation Current by a Contactless Photoconductivity Decay Method*, 18th IEEE Photovoltaic Specialists Conf. Las Vegas **1985**.
- [40] T. Trupke, R. Bardos, M. Schubert, W. Warta, *Appl. Phys. Lett.* **2006**, *89*, 44107.